Chapter 4
Gain Scheduled H_∞ Control of Wind Turbines for the Entire Operating Range

Fernando A. Inthamoussou, Fernando D. Bianchi, Hernán De Battista and Ricardo J. Mantz

Abstract Two different operating modes can be clearly identified in wind turbine control systems. In low wind speeds, the main control objective is the energy capture maximization, whereas in high wind speeds it is desired to regulate turbine power and speed at their rated values. The fulfillment of these different control objectives implies the transition through low controllability operating conditions that impose severe constraints on the achievable performance. The control task is usually tackled using two separate controllers, one for each operating mode, and a switching logic. Although satisfactory control solutions have been developed for low and high wind speeds, controller design needs refinement in order to improve performance in the transition zone. This chapter overviews a control scheme covering the entire operating range with focus on the transition zone. H_∞ and advanced anti-windup techniques are exploited to design a high performance control solution for both operating modes with optimum performance in the transition zone.

Keywords Anti-windup · Gain-scheduling control · H_∞ optimal control · Robust control · Wind turbines control

F.A. Inthamoussou · H. De Battista
CONICET and Instituto LEICI, Facultad de Ingeniería, Universidad Nacional de La Plata, CC 91 (1900), La Plata, Argentina
e-mail: intha@ing.unlp.edu.ar

H. De Battista
e-mail: deba@ing.unlp.edu.ar

F.D. Bianchi (✉)
Catalonia Institute for Energy Research, IREC, Jardins de Les Dones de Negre 1, 08930 Sant Adrià de Besòs, Barcelona, Spain
e-mail: fbianchi@irec.cat

R.J. Mantz
CIC and Instituto LEICI, Facultad de Ingeniería, Universidad Nacional de La Plata, CC 91 (1900), La Plata, Argentina
e-mail: mantz@ing.unlp.edu.ar

Nomenclature

β	Pitch angle
β_r	Pitch angle command
β_o	Optimum pitch angle
Θ	Torsion angle
λ	Tip-speed-ratio
λ_o	Optimum tip-speed-ratio
ρ	Air density
τ	Time constant of the pitch actuator
Ω_g	Generator speed
Ω_N	Rated rotational speed
Ω_r	Rotor speed
B_r	Intrinsic rotor damping
B_s	Drive-train damping
C_P	Power coefficient
$C_{P_{\max}}$	Maximum power coefficient
J_g	Generator inertia
J_t	Rotor inertia
K_s	Drive-train stiffness
k_β	Torque-pitch gain
k_{gs}	Gain-scheduling gain
k_V	Torque-wind speed gain
N_g	Gear-box ratio
P_r	Rotor power
P_N	Rated power
R	Rotor radius
T_g	Generator torque
T_N	Rated torque
T_r	Aerodynamic torque
T_{sh}	Shaft torque
V	Wind speed
V_N	Rated wind speed
$\|G(s)\|_\infty$	Denotes the ∞-norm of the stable system with transfer function $G(s)$
$\bar{x}$	Denotes steady-state value of x
$\hat{x}$	Denotes variation with respect to the steady-state value of x
$\dot{x}$	Denotes dx/dt

4.1 Introduction

Wind turbines are highly complex dynamical systems. They are flexible, mechanical structures subjected to spatially and temporally distributed disturbances, with interconnected dynamics, poorly damped, with physical constraints, etc. Additionally, they are operated and controlled in different modes depending on the wind speed. The operational region of wind turbines can be divided into three regions. On the one side, at low wind speeds one finds the partial-load region, also called region 1, where the main control objective is energy capture maximization. A complementary objective in this region is to reduce, or at least not to amplify, the aerodynamic loads [1]. At the opposite side of the operational wind speed range there is region 3, the full-load region. The objective there is to keep the turbine at its rated operating point. In this region, mitigation of aerodynamic and mechanical losses is crucial for the useful life of the wind turbine. In between, there exists a transition region (region 2) where the objective is to achieve a smooth transition between power tracking and regulation. Therefore, controller performance is mainly assessed in terms of loads alleviation.

Wind turbine control has been traditionally addressed in two ways. In one way, a multivariable controller is designed to guarantee satisfactory performance along the whole wind speed envelope. Some problems like low controllability and poorly damped oscillations make this task very complicated, leading to solutions that are too conservative. In the other approach, two different controllers are designed to fulfill the control objectives for partial- and full-load, whereas a bumpless or anti-windup compensation avoids undesirable responses after controller switching. This is the control structure implemented in commercial wind turbines.

For many years, the focus has been on improving controller performance in low and high wind speeds. Less attention has been given to the transition region where there was not a clear control objective (see for instance [2–5]). However, the detrimental effects of loading is increasing as wind turbine size grows exponentially, thus moving the attention to load mitigation. That is why operation and controller performance in the transition zone, where the low controllability problems appear, is now receiving special interest in the wind industry and academy.

In this chapter, the two-controller approach with anti-windup compensation is revisited. A robust, gain-scheduling control scheme designed in the H_∞ optimal control framework is discussed in detail, with special focus on the performance in the transition zone. The turbine is controlled through the generator torque in the partial-load region, and through the pitch angle in the full-load one. An optimal anti-windup strategy is also included to achieve smooth operation in the transition region.

4.2 Wind Turbine Modeling

The energy captured by a wind turbine is a function of the rotor radius R, the wind speed V, the rotor speed Ω_r and the pitch angle β. More precisely, the rotor power can be expressed as

$$P_r(V, \beta, \Omega_r) = \frac{\pi \rho R^2}{2} C_P(\lambda, \beta) V^3, \tag{4.1}$$

where ρ is the air density and $\lambda = \Omega_r R/V$ is the tip-speed ratio. The efficiency of the energy capture is characterized by the power coefficient $C_P(\cdot)$. Figure 4.1 shows the power coefficient of the 5 MW NREL wind turbine benchmark reported in [6].

The rotor torque results from dividing the captured power by the rotational speed:

$$T_r(V, \beta, \Omega_r) = P_r(V, \beta, \Omega_r)/\Omega_r. \tag{4.2}$$

Modern wind turbines are complex mechanical systems exhibiting coupled translational and rotational movements. This complex dynamic behavior is in general well-captured by aeroelastic simulation codes such as the FAST (Fatigue, Aerodynamics, Structures, and Turbulence) code developed by the National Renewable Energy Laboratory (NREL) [7]. However, these models are not suitable for control design purposes. Simpler models including only a few oscillation modes are enough to design a control law. Here, for the sake of clarity, a two-mass model capturing just the first drive-train mode is used, whereas the unmodeled dynamics will be covered by additive uncertainty. The dynamical equations describing this model are

$$\begin{aligned}
\dot{\Theta} &= \Omega_r - \Omega_g/N_g, \\
J_t \dot{\Omega}_r &= T_r - T_{\text{sh}}, \\
J_g \dot{\Omega}_g &= T_{\text{sh}}/N_g - T_g,
\end{aligned} \tag{4.3}$$

where the state variables are the torsion angle Θ, the rotor speed Ω_r and the generator speed Ω_g. The model variables T_g and $T_{\text{sh}} = K_s \Theta + B_s(\Omega_r - \Omega_g)$ are the generator and shaft torques, respectively. The model parameters are the inertia J_t combining the hub and the blades, the generator inertia J_g, the gear box ratio N_g, and the shaft stiffness K_s and friction B_s coefficients. A representation of this two-mass model can be observed in Fig. 4.2.

In variable-speed wind turbines, the electrical generator is interfaced by a full or partial power converter that controls the generator torque T_g and decouples the rotational speed from the electrical grid. Since the power converter and generator dynamics are much faster than the mechanical subsystem, it can be assumed for

Fig. 4.1 Power coefficient C_P for a 5 MW variable-speed variable-pitch wind turbine [6]
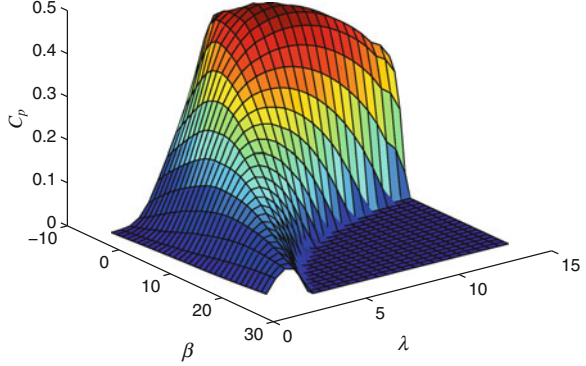
Fig. 4.2 Two-mass model describing the first drive-train mode
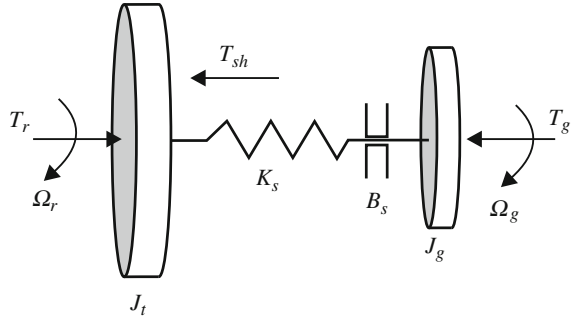
the purpose of this work that the torque reference of the power converter coincides with the electrical torque T_g imposed to the wind rotor. That is, it can be assumed that T_g is a control input.
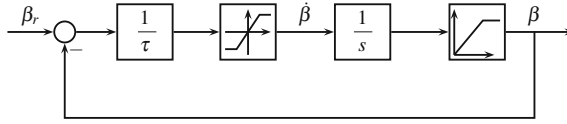
The pitch actuator is a highly nonlinear mechanic and hydraulic system [5]. For control-oriented purposes, it is usually modeled as a first-order low-pass filter with saturation in the amplitude β and rate of change $\dot{\beta}$. The pitch system is showed in Fig. 4.3. In the linear zone, the pitch actuator dynamics can be described by

$$\dot{\beta} = -\frac{1}{\tau}\beta + \frac{1}{\tau}\beta_r, \tag{4.4}$$

where τ is the time constant and β_r the pitch angle command.

The drive-train dynamics (Eq. 4.3) is highly nonlinear. This nonlinearity comes mainly from the aerodynamic torque (Eq. 4.2). For optimal control design, a linear representation of the system dynamics is necessary. With this aim, the aerodynamic torque is linearized around the operating point:

$$\hat{T}_r(\bar{V}, \bar{\beta}, \bar{\Omega}_r) = B_r(\bar{V}, \bar{\beta}, \bar{\Omega}_r)\hat{\Omega}_r + k_V(\bar{V}, \bar{\beta}, \bar{\Omega}_r)\hat{V} + k_\beta(\bar{V}, \bar{\beta}, \bar{\Omega}_r)\hat{\beta}, \tag{4.5}$$

Fig. 4.3 Pitch actuator model

where

$$B_r(\bar{V}, \bar{\beta}, \bar{\Omega}_r) = \left.\frac{\partial T_r}{\partial \Omega_r}\right|_{(\bar{V}, \bar{\beta}, \bar{\Omega}_r)}, \quad k_V(\bar{V}, \bar{\beta}, \bar{\Omega}_r) = \left.\frac{\partial T_r}{\partial V}\right|_{(\bar{V}, \bar{\beta}, \bar{\Omega}_r)},$$

$$k_\beta(\bar{V}, \bar{\beta}, \bar{\Omega}_r) = \left.\frac{\partial T_r}{\partial \beta}\right|_{(\bar{V}, \bar{\beta}, \bar{\Omega}_r)},$$

The bar over the variables denotes the corresponding values at the operating point, whereas the hat denotes deviations with respect to the operating point.

Substituting the linearized expression of the aerodynamic torque (Eq. 4.5) in the two-mass model (Eq. 4.3) and adding the linear model of the pitch system, the wind turbine becomes described, locally around a given operating point, by

$$\dot{x} = \begin{bmatrix} 0 & 1 & -1/N_g & 0 \\ -K_s/J_r & (B_r(\bar{V}, \bar{\beta}, \bar{\Omega}_r) - B_s)/J_r & B_s/J_r N_g & k_\beta(\bar{V}, \bar{\beta}, \bar{\Omega}_r)/J_r \\ K_s/J_g N_g & B_s/J_g N_g & -B_s/J_g N_g^2 & 0 \\ 0 & 0 & 0 & -1/\tau \end{bmatrix} x$$

$$+ \begin{bmatrix} 0 & 0 & 0 \\ k_V(\bar{V}, \bar{\beta}, \bar{\Omega}_r)/J_r & 0 & 0 \\ 0 & -1/J_g & 0 \\ 0 & 0 & 1/\tau \end{bmatrix} \begin{bmatrix} \hat{V} \\ T_g \\ \beta_r \end{bmatrix},$$

(4.6)

where $x = [\hat{\Theta} \; \hat{\Omega}_r \; \hat{\Omega}_g \; \hat{\beta}]^T$ is the state. The signal $\hat{V}$ is the wind speed acting as disturbance, and T_g and β_r are the control inputs.

4.3 Objectives and Control Scheme

A wind turbine normally works in different operating modes along the wind speed range [2]. These operating modes are illustrated in the power-wind speed curve of Fig. 4.4. The control objectives in these regions are substantially different. Below rated wind speed V_N (region 1), the objective is to capture as much energy as possible. In this case, the pitch angle is kept constant at its optimum value, whereas the rotational speed is varied in proportion to the wind speed by properly

Fig. 4.4 Wind turbine
operating regions
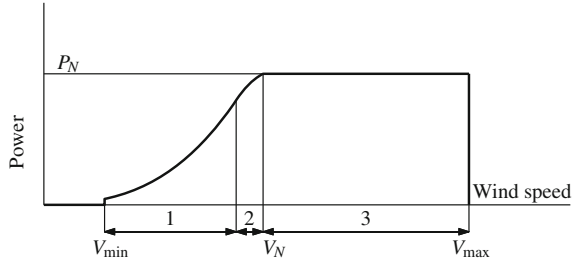
controlling the generator torque. Above rated wind speed (region 3), the objective
is to regulate the rotational speed and power at their rated values in order to protect
the wind turbine from high mechanical loads and excessive electrical currents. In
this region, the rotational speed is regulated acting on the pitch angle, whereas the
generator torque is kept constant at its rated value. Between these two regions,
there is a transition zone (region 2), in which the objectives and control structure
exhibit significant changes.

The operating locus of the wind turbine corresponding to the power-wind
strategy of Fig. 4.4 can be conveniently represented on a torque-rotational speed-
pitch angle space. This graph is shown in Fig. 4.5. In this figure, the projection of
this 3D curve onto the torque-rotational speed plane is also depicted. The three
operating regions can be easily identified.

- In region 1, the objective is energy capture maximization. Both the tip-speed
  ratio and the pitch angle should be maintained as close as possible to their
  optimum values: $C_P(\lambda_o, \beta_o) = C_{P_{max}}$. To this end, the generator torque is
  conventionally chosen to follow a quadratical relationship with the rotational
  speed, i.e.,

$$T_g = \left(\frac{\pi \rho R^5}{2\lambda_o^3} C_{P\max} \right) \Omega_g^2 = k_t \cdot \Omega_g^2. \tag{4.7}$$

- The transition region 2 commonly comprises two subregions. Once the rota-
  tional speed reaches the lower limit $\underline{\Omega}_{lim}$, the torque increases proportionally
  until the rated value T_N. Beyond the upper limit $\overline{\Omega}_{lim}$, the torque is maintained
  constant at the rated value. The objective in this region is to decouple as much
  as possible the control laws for regions 1 and 3.
- In region 3, the generator torque is kept constant at the rated value whereas the
  pitch angle is used to regulate the rotational speed.

In the literature, several control schemes covering the entire operating range
have been proposed. Basically, two approaches can be identified among the
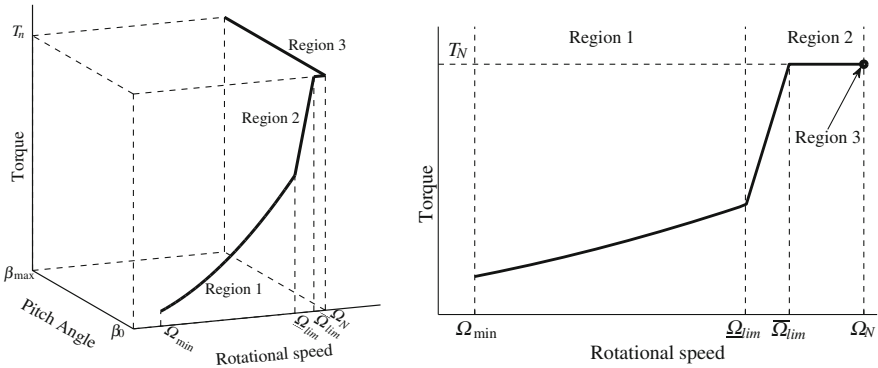
Fig. 4.5 Typical torque-rotational speed curve for a variable-speed variable-pitch wind turbine

proposals. In one of them, two different controllers for low and high wind speeds together with a switching strategy are designed (see for example, [8, 9]). Simple controllers can be used in each region at the cost of a bumpless or anti-windup compensation to reduce undesirable transients in the transition region. The other approach consists of just one control law (generally nonlinear) covering the whole operating envelope (see for example, [2, 5]). This approach yields more complex controllers, hence requiring more advanced control techniques. Furthermore, these controllers are usually more conservative and quite complex to implement.

The control scheme covering the entire operating range presented in this chapter is based on the first approach. It is sketched in Fig. 4.6. As previously mentioned, the generator torque follows the law in Eq. 4.7 below rated wind speeds. This control law is implemented as a look-up table, the LUT block in Fig. 4.6. While the rotational speed evolves well below rated (Ω_N), the pitch angle remains saturated at its lower limit β_o. Only after speed reaches Ω_N or approaches it fast enough, the pitch control becomes active. This pitch control is designed here using H_∞ optimal control tools. A gain scheduling technique is used to deal with the nonlinearity of the aerodynamic torque. In addition, anti-windup compensation is also included to smooth the transients in the transition region. This compensation is only active when the pitch angle saturates in order to recover optimally and softly the non saturated loop condition. The damping filter is commonly added to increase the damping of the drive-train oscillation mode. This filter is active in the three regions and it must be considered when the pitch controller is designed.

Figure 4.7 depicts the coefficients B_r, k_V and k_β as functions of wind speed over the operational wind speed range of the 5 MW wind turbine [6]. In particular, the intrinsic damping B_r and pitch gain k_β are of special interest since they affect the stability and performance of the closed loop system. To compensate for the nonlinearity in the pitch action, the inverse of the coefficient k_β (k_β^{-1}) is inserted in the loop. Besides, the intrinsic damping B_r is considered an uncertain parameter instead of a nonlinear function of the operating point. In this way, by canceling the nonlinearity in k_β and covering with uncertainty the nonlinearity in B_r, the
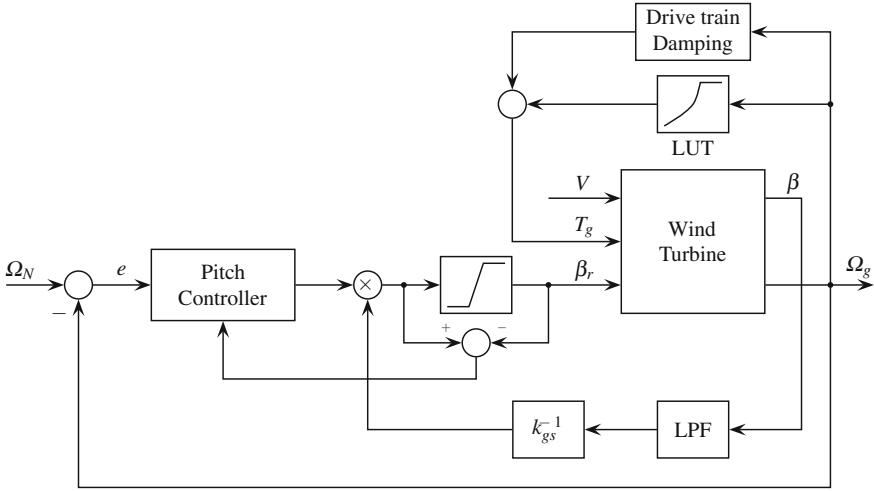
Fig. 4.6 Control scheme covering the entire operating range

rotational speed can be regulated with a linear time-invariant (LTI) controller. That is, an LTI controller designed for a given operating point can be used for the whole operating locus. To deal with the parameter uncertainty, H_∞ optimal control tools will be used.

To implement this control strategy, it is necessary to invert k_β, which is parameterized by wind speed. Recall, however, that wind speed in not measurable. To overcome this problem, the one-to-one correspondence between wind speed and pitch angle that exists in region 3 of the operating locus of Fig. 4.5 can be exploited. In fact, this one-to-one correspondence means that $\bar{\beta}$ suffices to uniquely determine the operating point in this region. Particularly, it means that k_β can be parameterized just in terms of $\bar{\beta}$. This allows computing k_β^{-1} as function of a measurable variable. To simplify this computation, the coefficient k_β can be approximated by

$$k_\beta(\bar{\beta}) = k_{\beta 0} k_{\text{gs}}(\bar{\beta})$$

The gain $k_{\beta 0}$ is k_β evaluated at operating point where the LTI controller is designed, whereas $k_{\text{gs}}(\cdot)$ is a second order polynomial of the form

$$k_{\text{gs}}(\bar{\beta}) = c_2 \bar{\beta}^2 + c_1 \bar{\beta} + c_0$$

computed by curve fitting. The values of $k_\beta / k_{\beta 0}$ and the approximation k_{gs} for the 5 MW NREL wind turbine can be seen in Fig. 4.8. To avoid loop interactions, the scheduling parameter $\bar{\beta}$ is obtained by passing the pitch angle through a low pass filter (LPF).

Before describing the control design, a brief review of H_∞ optimal control concepts is provided in the next section.

Fig. 4.7 Values of the
linearization coefficients B_r,
k_V and k_β in the entire wind
speed range
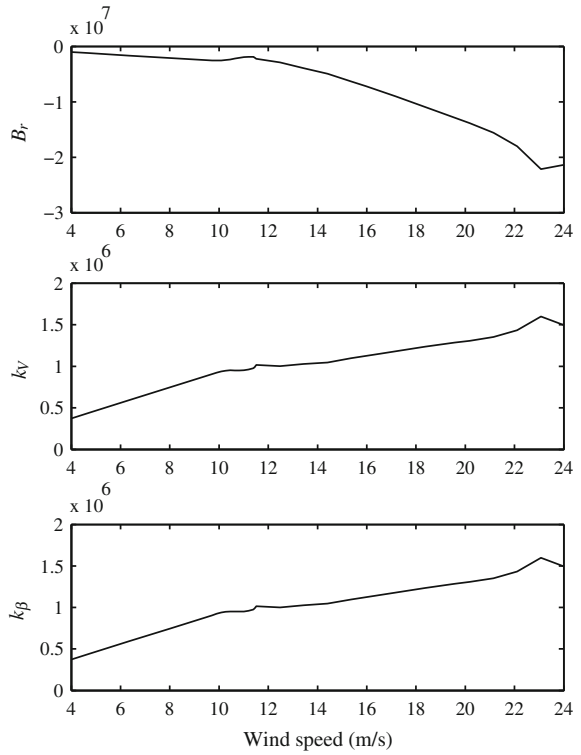
Fig. 4.8 Values of $k_\beta/k_{\beta 0}$ for
several wind speeds and the
second order polynomial
approximation
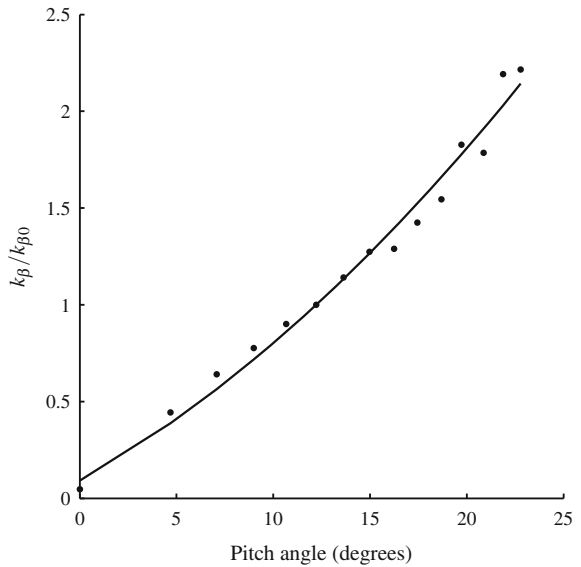
4.4 H_∞ Optimal Control Background

Consider an LTI system with the following state space realization

$$
\begin{aligned}
\dot{x} &= Ax + B_w w + B_u u \\
z &= C_z x + D_{zw} w + D_{zu} u \\
y &= C_y x + D_{yw} w + D_{yu} u
\end{aligned}
\tag{4.8}
$$

where $A \in \mathbb{R}^{n \times n}$, $D_{zw} \in \mathbb{R}^{n_z \times n_w}$ and $D_{yu} \in \mathbb{R}^{n_y \times n_u}$. The signal u is the control input and w is the disturbance. The signal y is the controlled variable and z is a fictitious output signal that serves to state the control objectives. The signal z is commonly named as the performance output.

It is assumed that system in Eq. 4.8 is stabilizable and detectable. That is, there exists a control law $u = K(s)y$ that stabilizes the closed loop system

$$
T_{zw}(s) = G_{zw}(s) + G_{zu}(s)K(s)(I + G_{yu}(s)K(s))^{-1}G_{yw}(s)
$$

with I the identity matrix and $G(s)$ the transfer function of the system in Eq. 4.8 partitioned as

$$
G(s) = \begin{bmatrix} G_{zw}(s) & G_{zu}(s) \\ G_{yw}(s) & G_{yu}(s) \end{bmatrix} = \left[\begin{array}{c|cc} A & B_w & B_y \\ \hline C_z & D_{zw} & D_{zu} \\ C_y & D_{yw} & D_{yu} \end{array} \right].
$$

The γ-suboptimal H_∞ synthesis problem consists in finding an internally stabilizing control law $u = K(s)y$ that guarantees an ∞-norm of the closed-loop transfer function from the disturbance w to the performance output z lower than γ. Being $T_{zw}(s)$ being the closed-loop transfer function from w to z, the control objective can be formalized as

$$
\|T_{zw}\|_\infty < \gamma,
\tag{4.9}
$$

where $\| \cdot \|_\infty$ denotes the infinity norm. For a stable system with transfer function $G(s)$, the ∞-norm is defined as

$$
\|G(s)\|_\infty = \max_\omega \sigma_{\max}(G(j\omega))
$$

where $\sigma_{\max}$ is the maximum singular value and ω is the frequency [10]. In other words, the ∞-norm is basically the maximum gain of the frequency response of the transfer function $G(s)$.

There are several solutions for the γ-suboptimal H_∞ synthesis problem, but the most popular nowadays is the formulation as an optimization problem with linear matrix inequalities (LMIs) constraints [11]. Considering a controller with a state-space realization

$$K(s) = \left[\begin{array}{c|c} A_k & B_k \\ \hline C_k & D_k \end{array}\right],$$

the controller matrices can be found by solving the following optimization problem:

minimize $\gamma(R, S, \hat{B}_k, \hat{C}_k, D_k)$,
subject to

$$\begin{bmatrix} AR + B_u\hat{C}_k + (\bigstar) & \bigstar & \bigstar \\ (B_w + B_y D_k D_{yw})^T & -\gamma I_{n_w} & \bigstar \\ C_z R + D_{zu}\hat{C}_k & D_{zw} + D_{zu}D_k D_{yw} & -\gamma I_{n_z} \end{bmatrix} < 0,$$

$$\begin{bmatrix} (SA + \hat{B}_k C_y) + (\bigstar) & \bigstar & \bigstar \\ (SB_w + \hat{B}_k D_{yw})^T & -\gamma I_{n_w} & \bigstar \\ C_z + D_{zu}D_k C_y & D_{zw} + D_{zu}D_k D_{yw} & -\gamma I_{n_z} \end{bmatrix} < 0,$$

$$\begin{bmatrix} R & I \\ I & S \end{bmatrix} > 0,$$

with ">" and "<" denoting positive and negative definite matrices, respectively, and $\bigstar$ represents the matrices needed to obtain a symmetric matrix.

After finding the positive definite matrices R and S and matrices $\hat{B}_k$, $\hat{C}_k$ and D_k, the controller matrices can be computed from

$$A_k = -(A + B_u D_k C_y)^T + \begin{bmatrix} SB_w + \hat{B}_k D_{yw} & C_z + D_{zu}D_k C_y \end{bmatrix}$$
$$\begin{bmatrix} -\gamma I & (D_{zw} + D_{zu}D_k D_{yw})^T \\ D_{zw} + D_{zu}D_k D_{yw} & -\gamma I \end{bmatrix}^{-1} \begin{bmatrix} (B_w + B_y D_k D_{yw})^T \\ C_z R + D_{zu}\hat{C}_k \end{bmatrix}$$
$$B_k = N^{-1}(\hat{B}_c - SB_u D_c),$$
$$C_k = (\hat{C}_k - D_k C_y R)M^{-T},$$

with $MN^T = I - RS$.

The optimization problem involved in the H_∞-synthesis can be effectively solved with available software such as Sedumi [12] and YALMIP [13]. It is also available as a command in the Robust Control Toolbox for Matlab. Therefore, the design process of an H_∞ optimal control requires only to put the control specifications in terms of the minimization of the norm in Eq. 4.9, i.e., to construct the
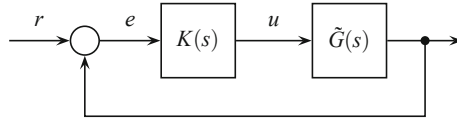
Fig. 4.9 Closed loop system with uncertain plant

augmented plant (Eq. 4.8) by selecting the performance output z and the disturbance w. More details about this process will be given in the next following sections.

One of the most common uses of H_∞-synthesis is the design of robust controllers. The dynamics of a system can be described by a model, but this description is always an approximation. There always exists discrepancy between system behavior and response predicted by the model, caused for example for changes in some parameters or unmodeled phenomena. To consider this situation, the system is described as a family of models in the form

$$\tilde{G}(s) = G_o(s) + W_\Delta(s)\Delta, \quad \|\Delta\|_\infty < 1, \tag{4.10}$$

where G_o is the nominal model and W_Δ is a filter describing the modeling error at different frequencies. Δ is an unknown LTI system with ∞-norm bounded by 1. It can be proved that the closed loop comprising system $\tilde{G}(s)$ and controller $K(s)$ (Fig. 4.9) is stable for all $\|\Delta\|_\infty < 1$ if the ∞-norm of the transfer function from r to u is lower than 1, i.e.,

$$\|K(s)(I + G(s)K(s))^{-1}\|_\infty < 1. \tag{4.11}$$

When a controller $K(s)$ ensures stability for all plants in the set in Eq. 4.10, it is said that the closed loop is robustly stable and Eq. 4.11 is the robust stability condition associated to the uncertainty representation in Eq. 4.10. Notice that there are other uncertainty representations, but Eq. 4.10 is one of the most commonly used (for more details see for example, [10]).

4.5 Wind Turbine Control Design

In this section, we present an H_∞ pitch controller. As said before, an anti-windup controller was added to avoid undesirable behavior caused by pitch saturation in the transition from region 1 to region 3. The controller is designed following a two-step process. First, the H_∞ pitch controller is designed disregarding the pitch saturation. Then, the anti-windup controller is designed for a suitable performance in the transition region.

4.5.1 H_∞ Optimal Pitch Control

As described in the previous section, the first step in the design of an H_∞ optimal control is to state the augmented plant. This implies stating the specifications in terms of the norm-minimization of the mapping between the performance output z and the disturbance w. Model uncertainty can be covered by properly choosing these signals, thus ensuring robust stability. Therefore, before describing the augmented plant, we find the model uncertainty representation to cover the variation of the parameter B_r and other errors caused by the approximation of the wind turbine behavior with a low-order model. The use of the scheduling gain $k_{gs}^{-1}(\bar{\beta})$ allows canceling the variation of the linearized aerodynamic torque with respect to the operating conditions. However, the variations in B_r are not so simple to compensate for, since they affect the eigenvalues of the linear model.

For control design purposes, the wind turbine can be modeled, after applying the scheduling gain in the control input, by the following parameter dependent transfer function

$$G(s) = \left[\begin{array}{cccc|c} 0 & 1 & -1/N_g & 0 & 0 \\ -K_s/J_r & (B_r(\bar{\beta}) - B_s)/J_r & B_s/J_r & k_{\beta 0}/J_r & 0 \\ K_s/J_g N_g & B_s/J_g N_g & -B_s/J_g N_g^2 & 0 & 0 \\ 0 & 0 & 0 & -1/\tau & 1/\tau \\ \hline 0 & 0 & 1 & 0 & 0 \end{array} \right].$$

Figure 4.10 shows the frequency response of this transfer function for several operating points in region 3. These results correspond to the 5 MW wind turbine previously mentioned. It can be seen that these variations can be covered by additive uncertainty of the form in Eq. 4.10 with the weighting function $W_\Delta(s)$ shown in the right plot of Fig. 4.10. In the uncertainty set, the scheduling gain errors caused by the polynomial approximation and the high-frequency unmodeled oscillation modes can also be covered.

In high wind speeds, the control objectives are the regulation of the rotational speed close to the rated value Ω_N and the reduction of the pitch activity to avoid high mechanical stresses. In the H_∞ optimal control framework, these objectives lead to the augmented plant of Fig. 4.11. In this case, the control input u is the pitch command and the controlled signal y is the rotational speed error $e = \Omega_N - \Omega_g$. Then, the performance signal is $z = [\tilde{e}, \tilde{\beta}_r]^T$ and the disturbance is the rotational set-point $w = \Omega_N$. Notice that the wind speed could also be considered as a disturbance. However, this would not improve the performance, but only increase the controller complexity.
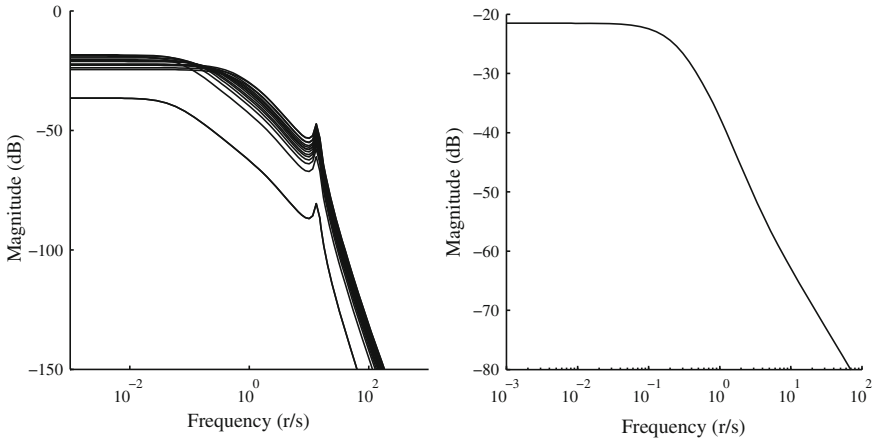
Fig. 4.10 *Left* frequency response of $G(s)$ corresponding to several operating points in region 3. *Right* weighting function W_A of the additive uncertainty representation Eq. 4.10
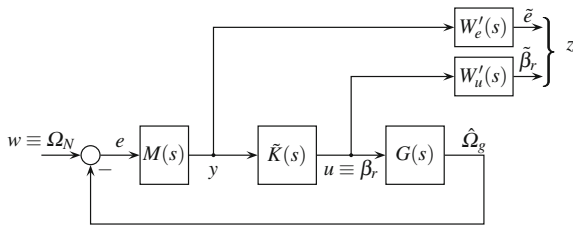
Fig. 4.11 Controller design setup augmented with weighting functions

The speed regulation results in the minimization of the low frequency components of the speed error $\tilde{e} = W'_e(s)(\Omega_N - \Omega_g)$, where

$$W'_e(s) = M(s)W_e(s) \tag{4.12}$$

with W_e a stable transfer function. If M includes integral action, the weight W_e can be a simple constant, such as,

$$M(s) = 1/s, \quad W_e = k_e.$$

The integral action ensures a zero steady-state error and penalizes the rotational speed error in low frequencies. Tracking error in high frequencies is not recommended because it would expose the wind turbine to excessive mechanical loads. The factorization in Eq. 4.12 is necessary for satisfying stabilizability conditions [10]. The controller actually applied to the wind turbine is
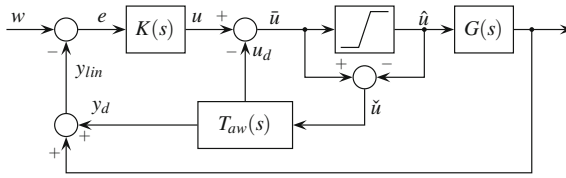
Fig. 4.12 Anti-windup compensation scheme

$$K(s) = M(s)\tilde{K}(s)$$

with $\tilde{K}(s)$ the controller produced by the optimization algorithm.

The weighting function $W_u(s)$ is a high pass filter such as

$$W_u(s) = k_u \frac{s/0.1\omega_u + 1}{s/\omega_u + 1}$$

with k_u and ω_u design parameters. This transfer function penalizes the high frequency components of the control signal, thus limiting the pitch activities. High frequency control action must be also avoided to prevent from rate pitch saturation. Since the modeling errors are covered by additive uncertainty, robust stability and the limitation of the pitch activity can be expressed as a constraint on the same closed loop transfer function. Therefore, the weighting function $W_u'(s)$ in Fig. 4.11 is the most restrictive function between $W_u(s)$ and $W_\Delta(s)$.

Notice that if the drive-train damping controller is considered, the plant $G(s)$ in Fig. 4.11 must include its dynamics in order to guarantee close loop stability.

Since the pitch controller is only active in region 3, an anti-windup controller is necessary to ensure good behavior during the transition from region 1 to region 3. With this purpose an optimal anti-windup controller is added. This controller is not shown in Fig. 4.6 for a matter of clarity. The anti-windup controller connection is shown in Fig. 4.12.

4.5.2 Anti-windup Compensation

In the control scheme of Fig. 4.6, the pitch controller will be in saturation during the low wind speed intervals. So, anti-windup compensation is absolutely necessary. To achieve high performance compensation, the anti-windup scheme proposed by [14, 15] is adopted here. It can be seen in Fig. 4.12. This scheme offers a good trade-off between stability margin and smooth recovery from saturation.

As can be seen in Fig. 4.12, the anti-windup compensator produces two terms: y_d acting on the controller input and another u_d acting on the control output. It can
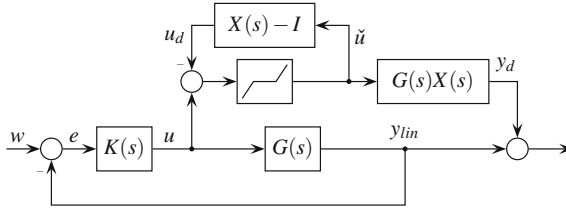
Fig. 4.13 Equivalent representation of the anti-windup compensation scheme in Fig. 4.12

be proved, after some system manipulations, that the block diagram in Fig. 4.13 is equivalent to the scheme in Fig. 4.12 by defining

$$\begin{bmatrix} u_d(s) \\ y_d(s) \end{bmatrix} = T_{\text{aw}}(s)\check{u}(s) = \begin{bmatrix} X(s) - I \\ Y(s) \end{bmatrix} \check{u}(s), \tag{4.13}$$

where X and Y are the coprime factors of G, i.e., $G = X^{-1}Y$. Therefore, the anti-windup compensator can be expressed as

$$T_{\text{aw}}(s) = \left[\begin{array}{c|c} A + B_u F & B_u \\ F & 0 \\ \hline C_y + D_{yu}F & D_{yu} \end{array} \right] \tag{4.14}$$

where F is chosen for $A + B_u F$ to be Hurwitz.

In this way X must be designed to ensure the closed-loop stability of $X - I$ and the deadzone nonlinear operator. At the same time, X must be designed to minimize the effect of y_d on the controlled variable. It can be proved that using the Lyapunov function $V(x_{\text{aw}}) = x_{\text{aw}}^T P x_{\text{aw}} > 0$ and forcing

$$\dot{V}(x_{\text{aw}}) + y_d^T y_d - v u^T u < 0, \tag{4.15}$$

with x_{aw} the state of the system T_{aw}, the previously mentioned objectives are satisfied. Because of the sector boundedness of the dead-zone nonlinearity, the following condition is satisfied

$$2\check{u}^T U^{-1}(u - Fx_{\text{aw}} - \check{u}) \geq 0, \tag{4.16}$$

with U a diagonal matrix.

After some mathematical manipulations, the problem of finding an anti-windup compensator is reduced to a state feedback F satisfying the following optimization problem with LMI constraints:

minimize $v(Q, U, L)$,
subject to

$$\begin{bmatrix} (AQ + B_uL) + (\star) & B_uU - QF^T & 0 & QC_y^T + L^TD_{yu}^T \\ \star & -2U & I & UD_{yu}^T \\ \star & \star & -vI & 0 \\ \star & \star & \star & -vI \end{bmatrix} < 0,$$

$$Q = Q^T > 0,$$

where $\star$ are inferred by symmetry. The state feedback gain is then obtained as $F = LQ^{-1}$ (see [16] for more details).

4.6 Results

The system behavior was evaluated by simulation on the 5 MW NREL wind turbine benchmark [6]. Simulations were performed in the FAST/Simulink®/ Matlab® environment. A more complete 16 degrees-of-freedom model available in FAST [7] was used as a way to assess the robustness of the proposed control scheme against unmodeled dynamics. The wind turbine data are given in Table 4.1, whereas the limit values of the operating locus are listed in Table 4.2.

The pitch controller was designed according to the control setup in Fig. 4.11 with

$$W'_e(s) = M(s)W_e(s) = \frac{1}{s}k_e, W'_u = k_u \frac{s/0.1\omega_u + 1}{s/\omega_u + 1}$$

where $k_e = 0.3$, $\omega_u = 50$ and $k_u = 0.25$. The frequency response of the weights W'_e, W_Δ and W_u are shown in Fig. 4.14. Remember that W'_u must be more demanding than W_u and W_Δ at every frequency. So, as can be seen in Fig. 4.14, it suffices to choose $W'_u = W_u$.

The ∞-norm of the closed loop transfer function T_{zw} resulted in 0.977. In particular, the norm of the transfer function from Ω_N to the control signal β, i.e.,

$$||K(I + KG)^{-1}||_\infty = 0.972.$$

As the norm is lower than 1, stability against covered modeling errors is guaranteed.

Table 4.1 Wind turbine parameters

Parameter value	Description
$P_N = 5.5967$ MW	Rated power
$N_p = 3$	Blades number
$R = 63$ m	Rotor radius
$N_g = 97$	Gear box ratio
$B_s = 6{,}210$ KNm/(r/s)	Drive-train damping
$J_r = 38{,}759{,}227$ kgm^2	Rotor inertia
$J_g = 534.2$ kgm^2	Generator inertia
$K_s = 867{,}637$ KN/r	Drive-train stiffness
$V_{\min} = 3$ m/s	Cut-in wind speed
$V_{\max} = 25$ m/s	Cut-out wind speed
$\beta_{\min} = 0°$	Minimum pitch angle
$\beta_{\max} = 30°$	Maximum pitch angle
$|\dot{\beta}|_{\max} = 10°/s$	Maximum pitch rate
$\Omega_N = 1{,}173.7$ rpm	Rated speed
$T_N = 43093.55$ Nm	Rated torque

Table 4.2 Operating curve values

Parameter description	Value
$V_{\min}$	3 m/s
$V_{\max}$	25 m/s
$\underline{\Omega}_{\lim}$	1,079 rpm
$\overline{\Omega}_{\lim}$	1,115 rpm
Ω_N	1,173.7 rpm
T_N	43,093.55 Nm

**Fig. 4.14** Weight functions used in the pitch control design
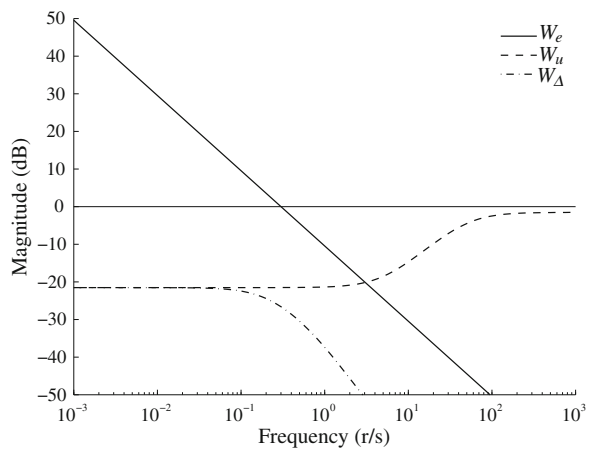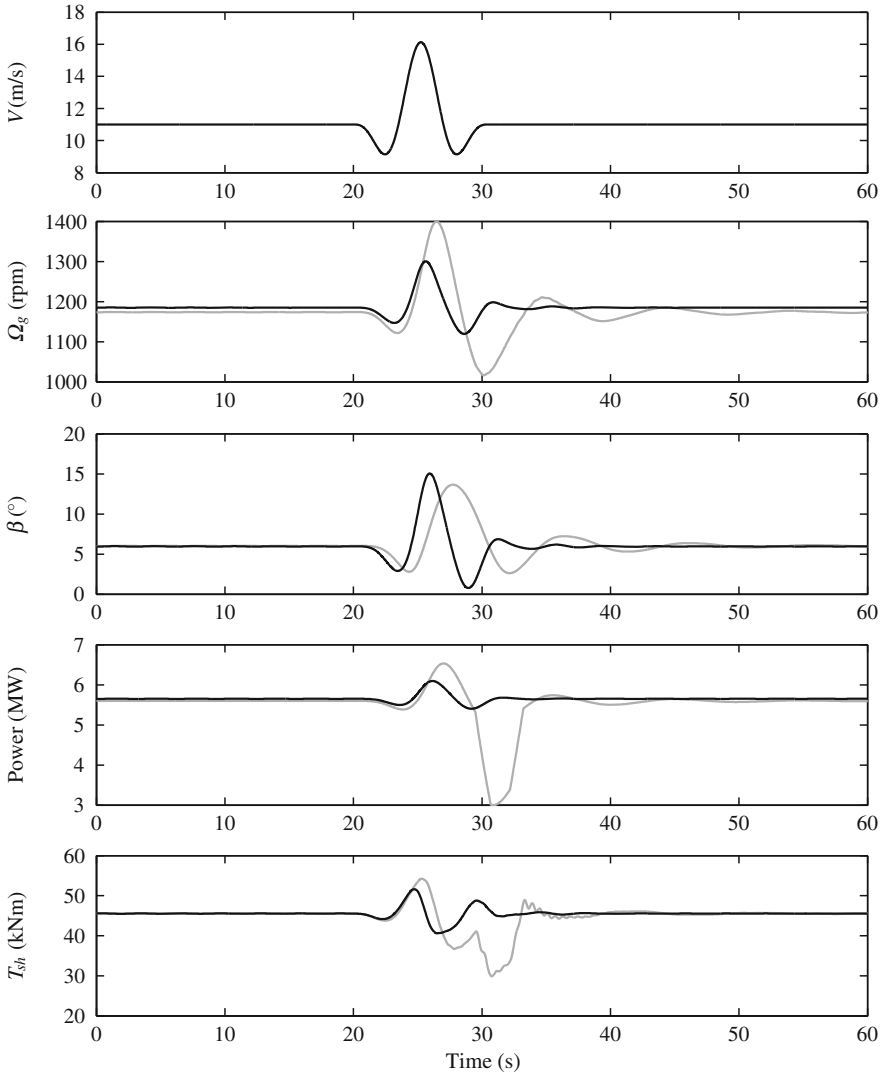
Fig. 4.15 System response to a wind gust profile. *Gray lines* PI controller, *black lines* H_∞ controller

After designing the pitch controller, the anti-windup compensation was computed by solving the optimization problem described in Sect. 5.2. The optimization problems for obtaining the H_∞ controller and the anti-windup compensation were solved using the Robust Control Toolbox for Matlab, Sedumi [12] and YALMIP [13].

For the sake of comparison, a classical gain-scheduled PI controller was also implemented and simulated. This PI, widely used in the literature as benchmark
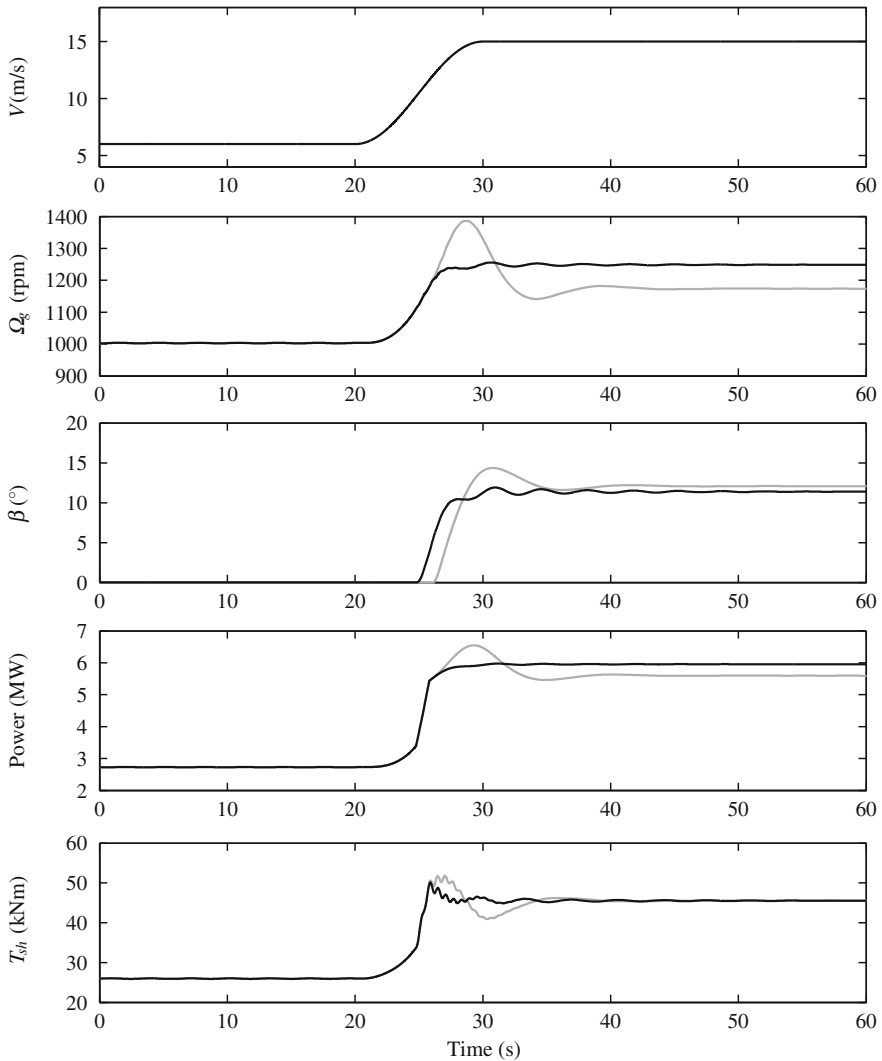
Fig. 4.16 System response to a wind rise profile. *Gray lines* PI controller, *black lines* H_∞ controller

controller, was designed following the guidelines in [6, 17]. Basically, the PI controller was tuned as in [6] after linearizing the wind turbine model at the operating point $(\bar{V}, \bar{\beta}, \bar{\Omega}_r) = (11.4\,\text{m/s}, 0, 12.1\,\text{rpm})$. The controller gains were calculated to achieve appropriate damping (0.7) and natural frequency (0.6 rad/s) [17]. As the controller ensures the desired behavior only at the design operating point, a pitch-dependent gain is applied to compensate for the nonlinear rotor torque. This gain is a function of β obtained by fitting the values of k_β along the
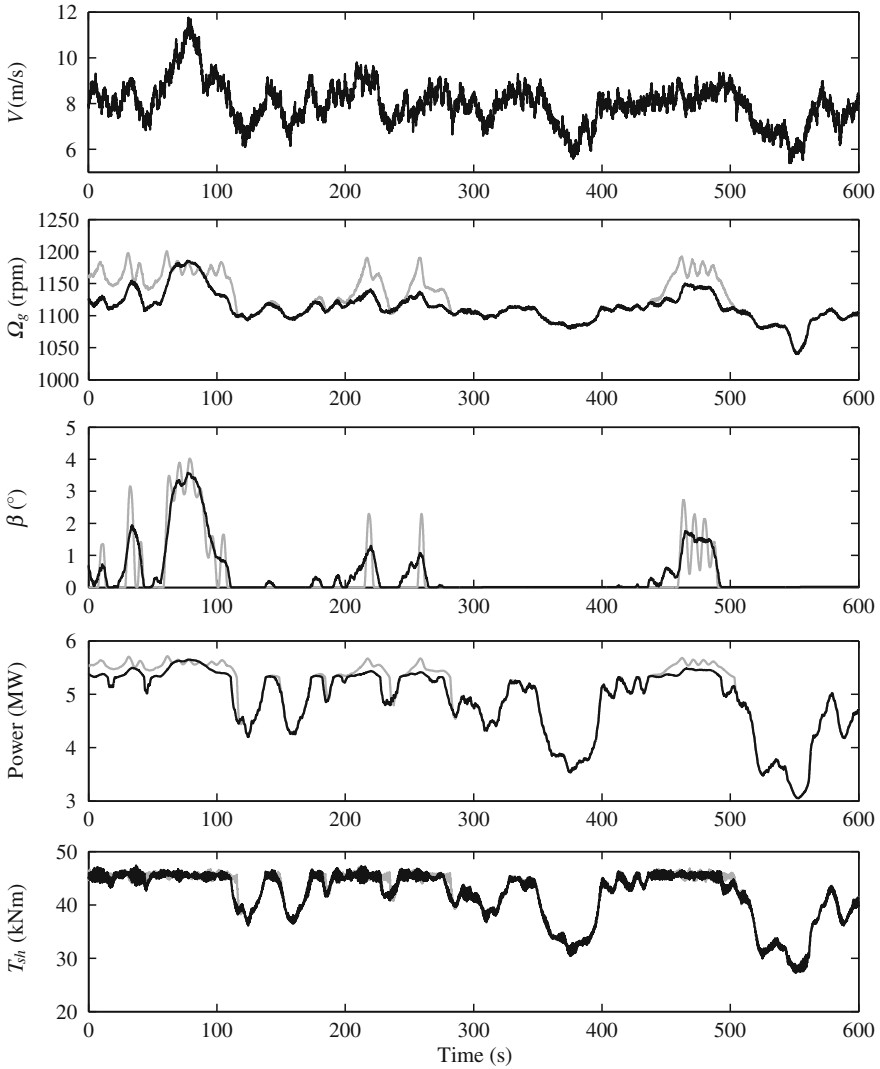
Fig. 4.17 System response to a realistic wind profile. *Gray lines* PI controller, *black lines* H_∞ controller

operating locus. In addition, a classical anti-windup compensation was added to improve the transient between regions 1 and 3. The PI tuning constants are $K_P(\beta = 0) = 0.01882681$ s, $K_I(\beta = 0) = 0.008068634$. The function that makes the gain scheduling is $f(\beta) = 1/(1 + \beta/\beta_k)$, where β is the pitch angle and $\beta_k = 6.30236$ is the blade pitch angle when the rotor power has doubled. The generator torque control is the same as in the H_∞ approach.

Three scenarios were simulated to assess the control performance. The first scenario is aimed at evaluating the performance of the controllers in region 3. To this end, the wind gust suggested in the IEC 61400-1 standard was used. This gust is very pitch demanding. The second scenario is mainly intended to assess the performance of the anti-windup compensator, i.e., the performance in the transition region. To this end, the wind rise proposed also in IEC 61400-1 standard was used. The last scenario illustrates the behavior of the controller under a realistic wind speed profile.

The simulation results obtained in the first scenario are presented in Fig. 4.15. As can be seen, the pitch controllers are always active. The H_∞ controller achieves better speed regulation with lower pitch activity than the PI controller. The speed overshoot is 16.86 % in the H_∞ case and 19.25 % in the PI case. Additionally, the H_∞ controller offers smoother responses in output power and shaft torque.

The results obtained in the second scenario are shown in Fig. 4.16. The wind profile rising from 6 to 13 m/s in 10 s makes the wind turbine to operate along the three regions. Again, it can be seen that the H_∞ controller achieves a better speed regulation with less pitch activity. Note that H_∞ with the anti-windup starts pitching the blades a bit before the PI with classical anti-windup does. The speed overshoot is 25.49 % in the H_∞ case and 32.96 % in the PI case. Like in the first scenario, the H_∞ controller offers smoother responses in output power and shaft torque.

The results for the last scenario are shown in Fig. 4.17. The 10 min wind speed field was generated with Turbsim [18]. The 8 m/s mean wind speed was selected so that the wind turbine operates in all the three operating regions, but most of the time in the transition one. It can be seen in the figure that the H_∞ controller achieves better speed regulation with significant less pitch activity.

4.7 Conclusion

This chapter presents a robust H_∞ pitch control design for variable-pitch variable-speed wind turbines operating along the entire wind speed range.

The main nonlinearities of the wind turbine dynamics are either canceled by inversion or covered with uncertainty so that an LTI H_∞ controller designed for a given operating point can be applied to the whole operating locus. The controller design guarantees robustness against unmodeled dynamics, cancelation errors and parameter uncertainties.

The system behavior was assessed by numerical simulations of a high-order wind turbine benchmark under three very demanding scenarios. Under these scenarios the H_∞ controller achieves better speed regulation with lower pitch activity than classical PI control. This lower pitch activity leads to lower mechanical stress spreading the wind turbine lifetime and also resulting in softer output power.

4.8 Future Research

The conservativeness inherent to the applied linearization, particularly due to the low-frequency uncertainty, can be eliminated by replacing the LTI design with the linear parameter varying (LPV) one. At the cost of a bit more complex implementation, better results particularly in speed regulation can be obtained. The complexity of the controller can be increased in order to consider more specifications as attenuating additional oscillation modes by adding more sensing signals.

References

1. Bossanyi EA (2003) Wind turbine control for load reduction. Wind Energy 6(3):229–244
2. Bianchi FD, De Battista H, Mantz RJ (2010) Wind turbine control systems: principles, modelling and gain scheduling design. Advances in industrial control. Springer-Verlag London Ltd., London
3. Muhando E, Senjyu T, Uehara A, Funabashi T (2011) Gain-scheduled H_∞ control for WECS via lmi techniques and parametrically dependent feedback part II: controller design and implementation. IEEE Trans Industr Electron 58(1):57–65
4. Munteanu I, Bratcu A, Cutululis N, Ceangă E (2007) Optimal control of wind energy systems: towards a global approach. Springer-Verlag London Ltd., London
5. Østegaard KZ, Stoustrup J, Brath P (2008) Linear parameter varying control of wind turbines covering both partial load and full load conditions. Int J Robust Nonlinear Control 19:92–116
6. Jonkman J, Butterfield S, Musial W, Scott G (2009) Definition of a 5-MW reference wind turbine for offshore system development. Technical report, NREL, 2009
7. Jonkman J (2013) NWTC computer-aided engineering tools (FAST). http://wind.nrel.gov/designcodes/simulators/fast/. Accessed 26 Aug 2013 (Last modified 27 Feb 2013)
8. Lescher F, Jing-Yun Z, Borne P (2006) Switching LPV controllers for a variable speed pitch regulated wind turbine. J Comput Commun Control 4:73–84
9. Yao X-j, Guo C-C, Li Y (2009) LPV H-infinity controller design for variable-pitch variable-speed wind turbine. In: Proceedings of the IEEE 6th international power electronics and motion control conference (IPEMC), pp 2222–2227, 2009
10. Sánchez Peña RS, Sznaier M (1998) Robust systems theory and applications. Wiley, New York
11. Gahinet P, Apkarian P (1994) A linear matrix inequality approach to H_∞ control. Int J Robust Nonlinear Control 4:421–448
12. Sturm J (1999) Using SeDuMi 1.02, a Matlab toolbox for optimization over symmetric cones. Optim Methods Softw 11–12:625–653
13. Löfberg J (2004) YALMIP: a toolbox for modeling and optimization in MATLAB. In: Proceedings of the CACSD conference, Taipei, Taiwan, 2004
14. Turner MC, Postlethwaite I (2004) A new perspective on static and low order anti-windup synthesis. Int J Control 77(1):27–44

15. Weston PF, Postlethwaite I (2000) Linear conditioning for systems containing saturating actuators. Automatica 36(9):1347–1354
16. Skogestad S, Postlethwaite I (2005) Multivariable feedback control: analysis and design. Wiley, UK
17. Hansen M, Hansen A, Larsen T, Øye S, Sørensen P, Fuglsang P (2005) Control design for a pitch-regulated, variable speed wind turbine. Technical report, RISØ, 2005
18. Kelley N, Jonkman B (2013) NWTC computer-aided engineering tools (TurbSim). http://wind.nrel.gov/designcodes/preprocessors/turbsim/. Accessed 28 Aug 2013 (Last modified 30 May 2013)